ADVANCED FUNCTIONAL MATERIALS

www.afm-journal.de

Hydrocarbons-Driven Crystallization of Polymer Semiconductors for Low-Temperature Fabrication of High-Performance Organic Field-Effect Transistors

*Yanlian Lei, Ping Deng, Qiaoming Zhang, Zuhong Xiong, Qinghua Li, Jiangquan Mai, Xinhui Lu, Xunjin Zhu, and Beng S. Ong**

While many high-performance polymer semiconductors are reported for organic field-effect transistors (OFETs), most require a high-temperature postdeposition annealing of channel semiconductors to achieve high performance. This negates the fundamental attribute of OFETs being a low-cost alternative to conventional high-cost silicon technologies. A facile solution process is developed through which high-performance OFETs can be fabricated without thermal annealing. The process involves incorporation of an incompatible hydrocarbon binder or wax into the channel semiconductor composition to drive rapid phase separation and instantaneous crystallization of polymer semiconductor at room temperature. The resulting composite channel semiconductor film manifests a nano/microporous surface morphology with a continuous semiconductor nanowire network. OFET mobility of up to about 5 $cm^2 V^{-1} s^{-1}$ and on/off ratio ≥ 10^6 are attained. These are hitherto benchmark performance characteristics for room-temperature, solution-processed polymer OFETs, which are functionally useful for many impactful applications.

1. Introduction

The potential of organic field-effect transistors (OFETs) as building blocks for generating low-cost, large-area electronic circuitries for next-generation electronics (e.g., lightweight, flexible displays, disposable electronics, etc.) stems from the expectation that they can be solution processed at room temperature under ambient conditions.[1] Solution processability permits utilization of high-throughput printing techniques (e.g., inkjet, screen, gravure, flexography, etc.) as manufacturing processes, leading to greatly reduced costs. Processing under ambient conditions avoids the needs for costly precautionary measures to isolate manufacturing from exposure to atmospheric oxygen and moisture, etc. Additionally, fabricating circuitries without engaging a postdeposition thermal annealing of channel semiconductors would be equally important as this is generally a slow process, which would otherwise reduce manufacturing speeds and increase costs. It is thus imperative and highly desirable that the channel semiconductor be fabricated at room temperature at ambient without thermal treatment to preserve the high-throughput process capability. Unfortunately, most high-performance OFETs, particularly those utilizing organic polymer semiconductors, require high-temperature annealing to improve channel semiconductor orderings for enhanced OFET performance.[2–7] Without thermal annealing, the OFET performance is generally less than satisfactory.[7–10]

Accordingly, achievement of high molecular orderings or crystallinity in the channel semiconductors to deliver performance characteristics that meet application requirements is one of the paramount issues in OFET manufacturing. Aside from thermal annealing, other crystallinity-enhancing strategies include solvent vapor annealing,[11,12] templating with prepatterned substrates,[13–16] etc., but most of these approaches are often either slow or costly. More recently, incorporation of inert guest polymers such as polystyrene, poly(methyl methacrylate), etc. into channel semiconductor compositions have been shown to facilitate semiconductor molecular ordering leading to enhanced OFET performances.[17–26] The best guest polymer appears to be polyacrylonitrile (PAN), which has profoundly boosted OFET mobility and current modulation of many donor–acceptor (D–A) polymer semiconductors.[24] The observed performance enhancements are directly linked to the formation of large crystalline charge transport domains facilitated by guest polymer PAN.

Dr. Y. L. Lei, Q. M. Zhang, Prof. Z. H. Xiong
School of Physical Science and Technology
Southwest University
Chongqing 400715, P. R. China
Dr. P. Deng, Dr. Q. H. Li, Dr. X. Zhu, Prof. B. S. Ong
Research Centre of Excellence for Organic Electronics and Department of Chemistry
Hong Kong Baptist University
Kowloon, Hong Kong SAR, P. R. China
E-mail: bong@hkbu.edu.hk
Dr. J. Mai, Dr. X. Lu
Department of Physics
The Chinese University of Hong Kong
New Territories, Hong Kong SAR, P. R. China
The ORCID identification number(s) for the author(s) of this article can be found under https://doi.org/10.1002/adfm.201706372.

DOI: 10.1002/adfm.201706372

 © 2018 WILEY-VCH Verlag GmbH & Co. KGaA, Weinheim

Nonetheless, the effectiveness of this approach could only be realized when a postdeposition high-temperature annealing is implemented. As of this date, it remains extremely challenging to attain high crystalline orders in the channel semiconductors for enhanced OFET performance without high-temperature thermal treatment.

We describe herein a facile solution process to achieve high crystalline orders in polymer channel semiconductors for OFETs at room temperature without postdeposition high-temperature thermal annealing. This process utilizes a hydrocarbon binder or wax (C_mH_{2m+2}) to assist room-temperature crystallization of D–A polymer semiconductors such as diketopyrrolopyrrole-dithienylthieno[3,2-b]thiophene polymer (DPP-DTT, **Figure 1**a). The result was a semiconductor/wax composite thin film impregnated with a long-ranged semiconductor nanowire network intercalating in a maze of nano/micropore structures. OFETs using a channel semiconductor of this nature had afforded field-effect transistor (FET) mobility of up to about 5 $cm^2\ V^{-1}\ s^{-1}$ and current on/off ratio of 10^6 and beyond, representing hitherto benchmark performance characteristics for room temperature, solution-processed polymer OFETs without thermal annealing. These OFET performance characteristics would be sufficiently useful for a wide variety of high-value applications including pixel-driving backplane electronics for large-area displays.[27] Likewise, similar encouraging results were also obtained with other D–A polymer semiconductors. Hydrocarbon binders that could be utilized for the present process include Parafilm wax and commodity hydrocarbon waxes such as household candle wax, lubrication waxes, and low molecular weight polyethylenes, etc. Accordingly, this represents an extremely efficient and universal fabrication process for creating potentially low-cost, impactful OFET circuitries for next-generation consumer electronics.

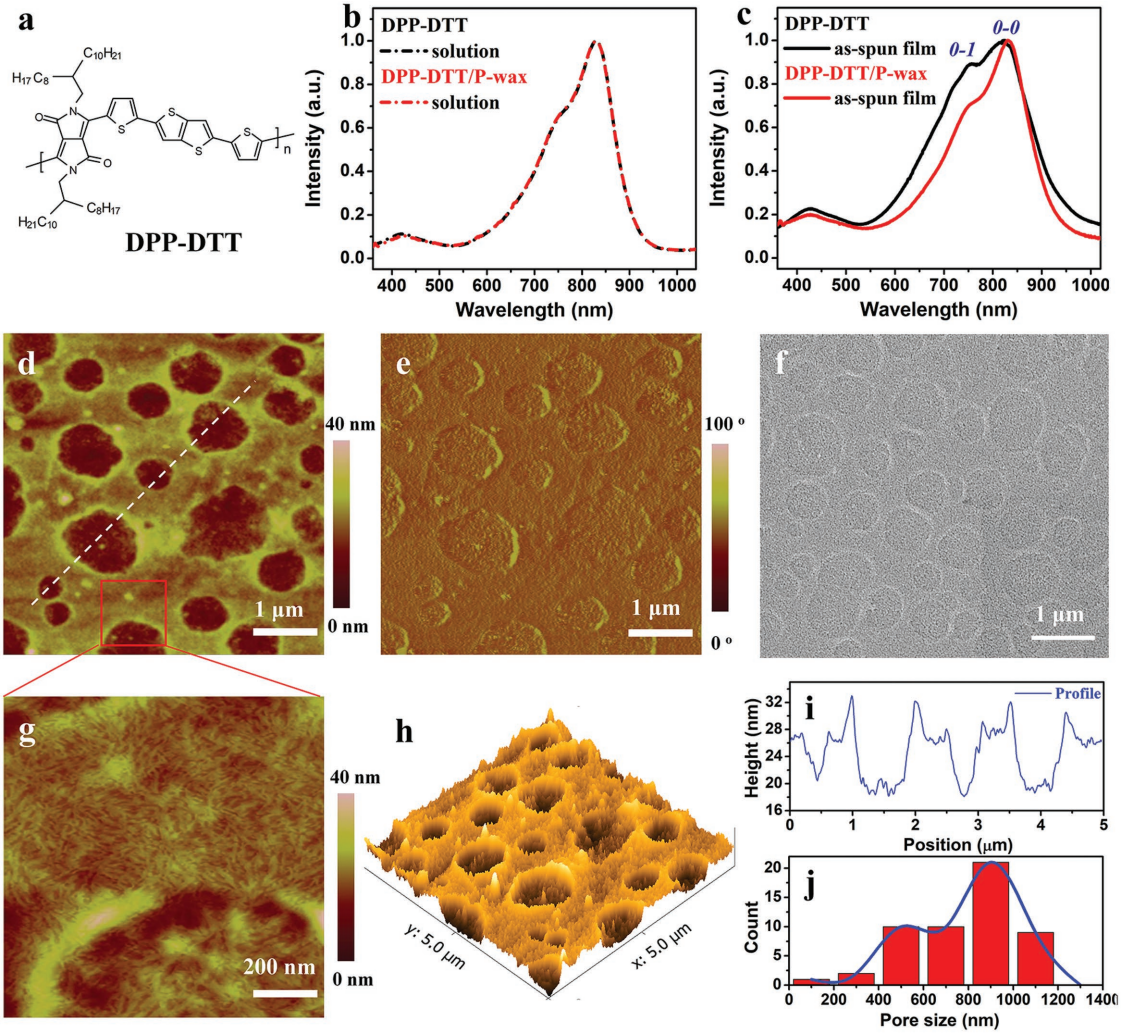

Figure 1. Nano/microporous structure formation in DPP-DTT polymer semiconductor/P-wax composite thin film. a) Chemical structure of DPP-DTT. b) Optical absorption spectra of neat DPP-DTT and DPP-DTT/P-wax (40/60) in dilute solutions and c) as-spun thin films; tapping model AFM, d) height image and e) phase image. f) SEM image of DPP-DTT/P-wax porous thin film. g) Enlarged AFM height image of selected area of panel (d). h) Corresponding 3D image of panel (d); i) Cross-sectional profile of AFM image along the dash line in panel (d); j) Distribution of pore size extracted from a large area of SEM image (≈10 × 10 μm^2).

© 2018 WILEY-VCH Verlag GmbH & Co. KGaA, Weinheim

2. Results and Discussion

The present process involved incorporation of a nonpolar, incompatible hydrocarbon wax into the coating solution to force phase separation and crystallization of polar D–A polymer semiconductors such as DPP-DTT upon solution deposition on a substrate. Specifically, when a solution of DPP-DTT and a hydrocarbon wax such as Parafilm M (henceforth referred to as P-wax) in a suitable solvent such as 1,2-dichlorobenzene (DCB) was deposited on a suitable substrate, rapid phase separation and instantaneous crystallization of DPP-DTT occurred at room temperature. The degrees of crystallinity of DPP-DTT in the resulting semiconductor/wax thin film depended very much on the proportion of DPP-DTT to P-wax in the coating solution. A 40/60 by weight of DPP-DTT/P-wax composition was found to optimal for FET performance. The addition of P-wax to the DPP-DTT solution also helped eliminate the solution gelling complications commonly observed with D–A polymer semiconductor solutions, thus enabling facile solution fabrication techniques such as high-throughput printing or coating.

In UV–vis absorption spectra, both the neat DPP-DTT and DPP-DTT/P-wax (40/60) solutions displayed essentially identical spectral features (Figure 1b), indicating that the electronic transitions of DPP-DTT were not affected by the presence of P-wax. On the contrary, the as-spun thin films of neat DPP-DTT and DPP-DTT/P-wax clearly manifested stark differences in absorption features (Figure 1c). Specifically, the neat DPP-DTT thin film showed much broader absorptions than those of DPP-DTT/P-wax film. The latter also exhibited a slight bathochromatic shift (≈8 nm) with a significantly enhanced *0-0*/*0-1* absorption band ratio attributable to stronger π–π stacking of DPP-DTT in the composite film.[28–30] These results lend supports to the role of P-wax in facilitating the π–π interactions of DPP-DTT polymer chains in as-spun thin films.

Using tapping-mode atomic force microscopy (AFM) and scanning electron microscopy (SEM), we observed some noteworthy and interesting morphological and microstructural features in the DPP-DTT/P-wax (40/60) composite films. Figure 1d (AFM height image) showed isolated nano/micropore structures randomly distributed throughout the film. This was quite different from that of DPP-DTT-only thin film, which showed a relatively uniform, pore-free morphology (Figure S1, Supporting Information). The formation of nano/micropore structures in the composite film was confirmed by SEM analysis (Figure 1f). The pore size ranges from nanometers to over 1 μm in diameter with a distribution peaking around about 900 nm (Figure 1j). The depth of the pores as measured from the cross-sectional profile of AFM image (dash line, Figure 1d) was ≈10–15 nm (see Figure 1i) in a 15–20 nm thick composite film. These nano/micropores were of a "well" shape structure with an outer rim (Figure 1h) protruding 3–5 nm above the surface of the film as measured from the cross-sectional profile. More importantly, a continuous DPP-DTT semiconductor nanowire network could visibly be seen to intercalate in these nano/micropore structures (Figure 1d,g).

The formation of nano/microporous semiconductor film was the result of phase separation of DPP-DTT polymer and P-wax upon solution deposition. A schematic representation of phase separation, nano/micropore, and nanowire network formation in the DPP-DTT/P-wax composite film is depicted in **Figure 2**. Specifically, solvent (DCB) evaporation from the cast film induced phase separation leading to P-wax/DCB nanodroplet and DPP-DTT nanowire formation (Figure 2a). This was followed by coalescence of P-wax nanodroplets to form larger microdroplets and continued growth of DPP-DTT nanowires to a continuous nanowire network (Figure 2b); subsequent cooperative forces of capillary effect from the DPP-DTT nanowire network and the coffee ring effect of DCB evaporation from P-wax/DCB nano/microdroplets at the surface of film resulted in the formation of nano/micropore structures (Figure 2c,d). The walls of these nano/micropores were presumably composed of P-wax as strong phase contrasts around the pores were noted in the phase image (Figure 1e), and that the nanowires were essentially DPP-DTT polymer since soaking the composite DPP-DTT/P-wax film in a hydrocarbon solvent (e.g., hexane and cyclohexane) could readily remove P-wax but not nanowire network.

The microstructural features and molecular packing behaviors in as-spun neat DPP-DTT and DPP-DTT/P-wax (40/60) composite films were investigated by grazing-incidence X-ray diffraction (GIXD) analysis. As shown in 2D GIXD mapping, both neat DPP-DTT (**Figure 3**a) and DPP-DTT/P-wax (Figure 3b)

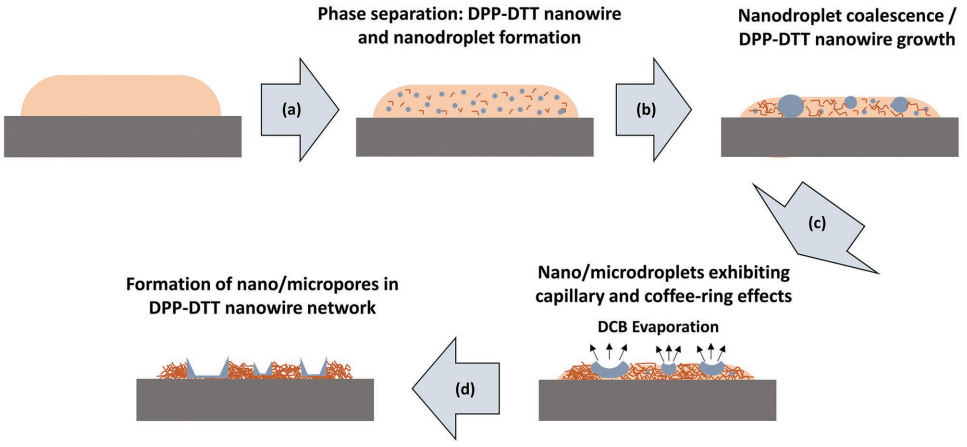

Figure 2. Schematic illustration of formation of nano/microporous DPP-DTT nanowire network thin film.

© 2018 WILEY-VCH Verlag GmbH & Co. KGaA, Weinheim

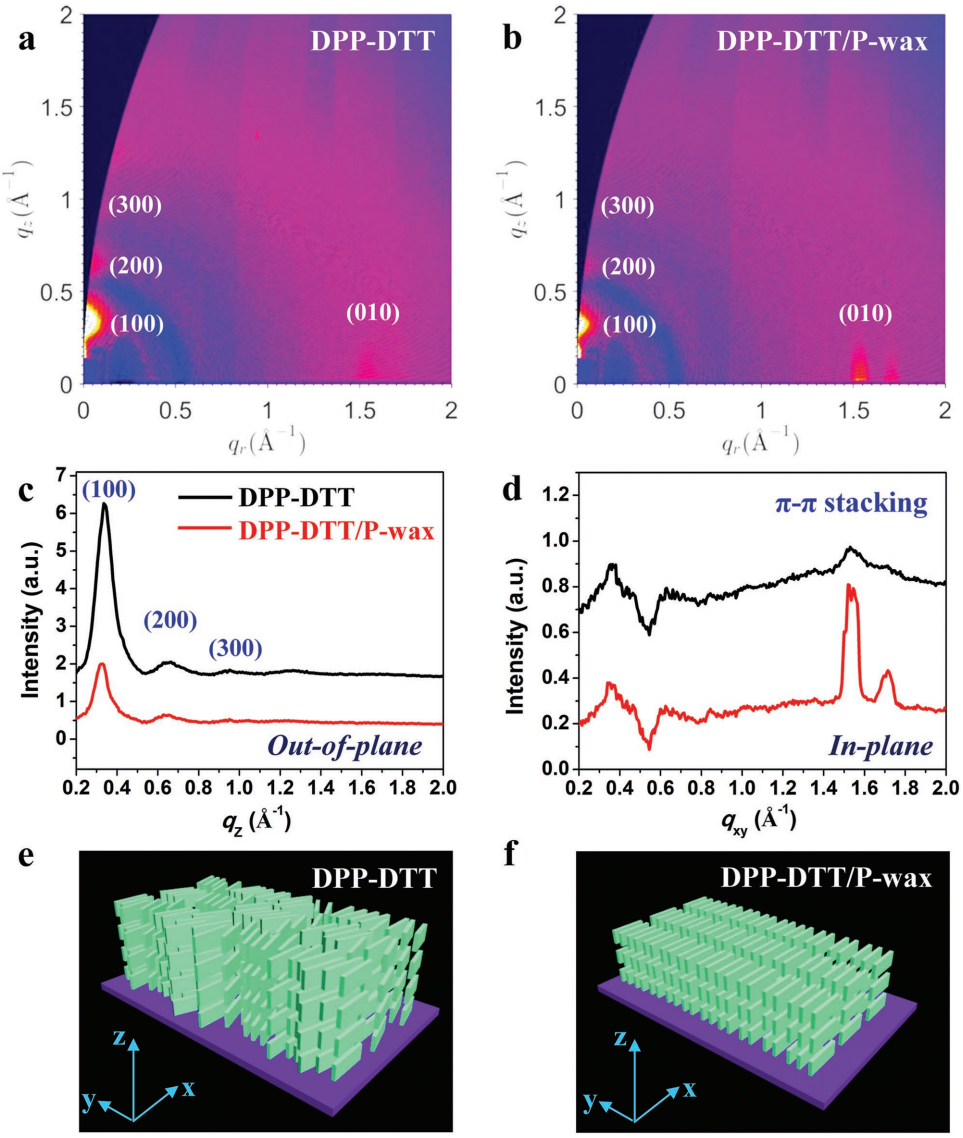

Figure 3. Molecular ordering in as-spun DPP-DTT neat and DPP-DTT/P-wax (40/60) composite films. 2D GIXD patterns of a) neat DPP-DTT thin film and b) DPP-DTT/P-wax composite thin film; c) out-of-plane and d) in-plane profiles extracted from 2D GIXD data; schematic illustrations of molecular arrangement in e) neat DPP-DTT thin film and f) DPP-DTT/P-wax composite thin film.

films displayed distinct interchain lamellar (100, 200, and 300) and π–π stacking (010) reflections. The π–π stacking reflection of DPP-DTT/P-wax film was substantially more intense than that of neat DPP-DTT film, reflecting much stronger π–π interactions in the DPP-DTT/P-wax film, thus higher crystalline orders. In the out-of-plane profile of GIXD (Figure 3c), both films exhibited strong (100) reflections with no observable signs of (010) reflections, while in the in-plane profiles (Figure 3d), the π–π stacking reflections were clearly noted. These observations unequivocally supported an edge-on orientation for the lamellar structures in both neat and composite films. The fact that the in-plane π–π stacking peak of DPP-DTT/P-wax film was much stronger than that of neat DPP-DTT film was a definitive manifestation of strong π–π stacking interactions, thus higher crystalline orders in the DPP-DTT/P-wax composite film. This was particularly true in view of the fact that the film thickness of DPP-DTT/P-wax film was more than three times thinner (≈15–20 nm vs ≈60 nm), and that DPP-DTT was also a minor component (40% by weight) in the DPP-DTT/P-wax composite film. This also explained for the observed somewhat lower intensity of the (100) reflection of the composite film in the out-of-plane GIXD (Figure 3c). Interestingly, two π–π stacking peaks at 1.53 and 1.71 $Å^{-1}$ were visually observed in the in-plane GIXD profiles of the two films (Figure 3d), suggesting two different π–π stacking interactions.[30] In addition, the weak π–π stacking peaks of neat DPP-DTT film were comparable in intensity with its (100) peak in the in-plane profile, suggesting absence of long-range π–π stacking orders. This was consistent with the rather randomly oriented small crystalline domains as schematically illustrated in Figure 3e. In sharp contrast, the π–π stacking peaks of DPP-DTT/P-wax composite film were much stronger with a small full-width at half maximum, indicative of

© 2018 WILEY-VCH Verlag GmbH & Co. KGaA, Weinheim

higher, long-range π–π stacking orders (Figure 3f). These results were in full agreement with the UV–vis spectral observations and AFM results, providing strong supports to our contention that nonpolar, incompatible hydrocarbon binders such as P-wax could enable creation of high-crystallinity polymer channel semiconductors for high-performance OFETs at room temperature.

To study OFET performance, a series of bottom-gate, top-contact OFETs with as-spun D–A polymer semiconductor/hydrocarbon wax composite thin films as channel semiconductors were fabricated on octadecyltrichlorosilane-treated Si/SiO_2 substrates (**Figure 4**a, inset) using gold source/drain electrodes. OFET characterization was performed at room temperature in

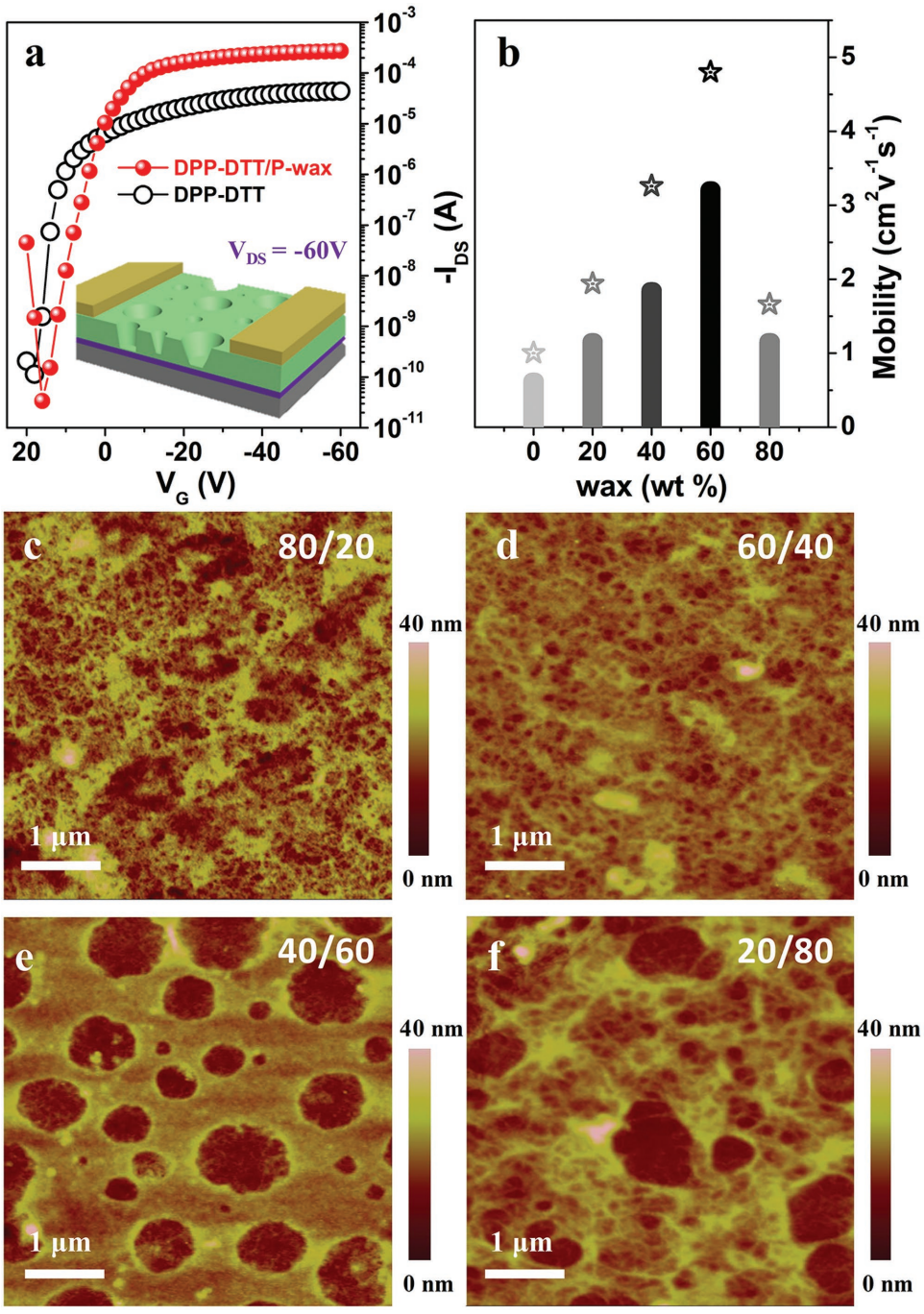

Figure 4. Charge transport properties of DPP-DTT/P-wax composite semiconductor films of various proportions. a) Representative transfer curves of OFETs with as-spun neat DPP-DTT and DPP-DTT/P-wax (40/60) composite channel semiconductors, inset is schematic of OFET configuration. b) Mobility distribution of OFETs with DPP-DTT/P-wax of various proportions with average and maximum mobility respectively represented by bars and stars. c–f) AFM height images of DPP-DTT/P-wax composite films of various proportions: c) DPP-DTT/P-wax = 80/20; d) DPP-DTT/P-wax = 60/40; e) DPP-DTT/P-wax = 40/60; and f) DPP-DTT/P-wax = 20/80.

© 2018 WILEY-VCH Verlag GmbH & Co. KGaA, Weinheim

ambient conditions, and the FET mobility was extracted from the transfer curves in the saturation regime (see details in the Supporting Information). While OFETs with neat DPP-DTT and DPP-DTT/P-wax channel semiconductors both exhibited typical p-type transport behaviors (see Figure 4a; Figure S3, Supporting Information), the DPP-DTT/P-wax-based OFETs exhibited significantly higher on-current and substantially lower off-current, demonstrating dramatically enhanced charge transport efficacy. The highest mobility was about 4.8 $cm^2 v^{-1} s^{-1}$ with the average being 3.2 $cm^2 v^{-1} s^{-1}$. This was over five times higher than that of those of OFETs utilizing neat DPP-DTT as channel semiconductor. Moreover, the hysteresis as manifested in the transfer curves was significantly reduced from ≈25 to 15 V for OFET devices with respectively neat DPP-DTT and DPP-DTT/P-wax semiconductors (Figure S4, Supporting Information). These results represent hitherto benchmark performance for polymer OFETs fabricated at room temperature without thermal annealing, and are potentially useful for a wide variety of next-generation electronic applications.

The effects of P-wax on charge transport properties of DPP-DTT/P-wax channel semiconductor were further investigated by varying the loading of P-wax in the composite films (20–80 by weight). The AFM images of DPP-DTT/P-wax composite films with varying loadings of P-wax are shown in Figure 4c–f, revealing profound differences in morphology. As can be noted, the nanopores were largely below 200 nm in size at low P-wax contents (Figure 4c,d), and grew with increasing P-wax loading to well over 1 µm in diameter when P-wax was around 60% by weight (Figure 4e). During this period of increasing P-wax loadings, DPP-DTT nanowires were formed and continued their growth to a continuous nanowire network intercalating in a maze of P-wax-walled nano/micropores when P-wax reached 60% by weight (Figure 4e). Beyond 60% P-wax loading, disruption and degradation of the continuous DPP-DTT nanowire network occurred (Figure 4f). This was obviously the consequence of drastically reduced DPP-DTT content and increased P-wax loading. The pronounced morphological changes correlated well with the charge transport properties of the composite channel semiconductors. As shown in Figure 4b, the FET mobility increased with P-wax loading, reaching its peak values at about 60% P-wax loading. Beyond 60% P-wax loading, a dramatic decrease in FET mobility resulted when the continuous DPP-DTT semiconductor network was disrupted (Figure 4f).

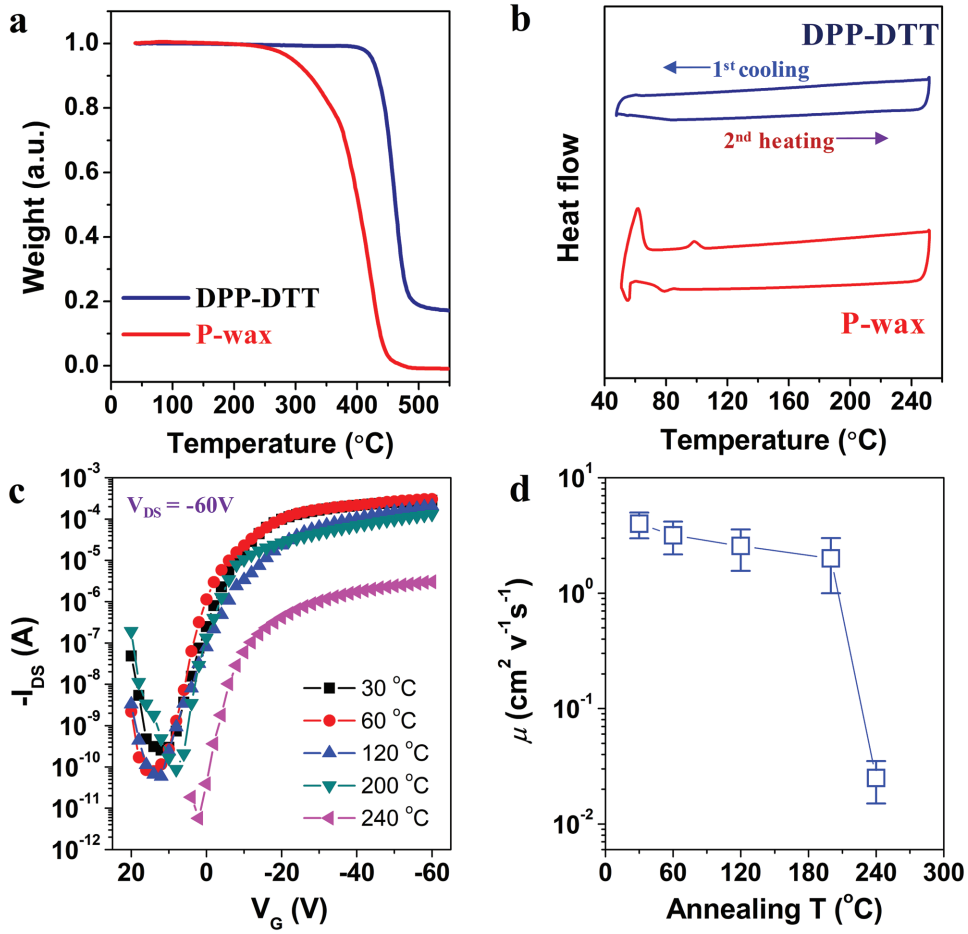

Figure 5. Thermal stability of OFETs with DPP-DTT/P-wax composite channel semiconductors. a) TGA and b) DSC profiles of DPP-DTT and P-wax materials. c) Transfer characteristics of OFETs with thermally treated DPP-DTT/P-wax composite channel semiconductors. d) OFET mobility versus treatment temperature from 30 to 240 °C.

© 2018 WILEY-VCH Verlag GmbH & Co. KGaA, Weinheim

These results were in agreement with the P-wax facilitated formation of a continuous DPP-DTT semiconductor nanowire network in providing efficient charge transport pathways in the DPP-DTT/P-wax composite channel semiconductor.

The thermal stability of the DPP-DTT/P-wax OFETs was studied using thermal gravimetric analysis (TGA) and differential scanning calorimetric (DSC) as these would be extremely important for practical applications. The decomposition temperatures of DPP-DTT and P-wax were measured to be respectively over 420 and 300 °C (**Figure 5**a), demonstrating excellent thermal stability of these materials. The melting point of P-wax was ≈100 °C, but no obvious phase transitions were observed for DPP-DTT within the temperature range of 40–250 °C (Figure 5b), most likely due to the high melting point of DPP-DTT over 250 °C.[31,32] Figure 5c shows the effects of thermal treatment on the FET properties of DPP-DTT/P-wax (40/60) OFETs at various temperatures (60, 120, 200, and 240 °C) for 10 min. While slight changes in transfer characteristics occurred after thermal treatment (from 60 to 200 °C), the FET mobility remained at over 2 cm^2 V^{-1} s^{-1} even at 200 °C (Figure 5d), showing excellent thermal stability of these OFETs. These results were consistent with the AFM observations, which showed no visible damages to the DPP-DTT nanowire network after thermal treatment at 200 °C (Figure S5a,b, Supporting Information). However, severe degradation in FET properties was noted when the OFETs were treated at 240 °C. At this temperature, visible damages to the continuous DPP-DTT semiconductor nanowire network were observed (Figure S5c,d, Supporting Information).

The hydrocarbon binder-driven room temperature molecular ordering/crystallization of D–A polymer semiconductors was shown to be general. The process had been applied with equal success to other D–A polymer semiconductors such as poly(diketopyrrolopyrrole-quaterthiophene) (DPP-QT; Figure S6a, Supporting Information) using P-wax and other hydrocarbon waxes such as household candle wax (Figure S6b, Supporting Information). Excellent DPP-QT/P-wax (60/40 wt%) OFETs were fabricated, displaying significantly better FET properties for the devices with DPP-QT/P-wax channel semiconductor (**Figure 6**a,b). The extracted mobility of DPP-QT/P-wax OFETs was 2.0 cm^2 v^{-1} s^{-1}, which was five times higher than those of OFETs with DPP-QT-only channel semiconductor (≈0.4 cm^2 V^{-1} s^{-1}). Likewise, similar enhancements in FET property were achieved with OFETs using DPP-DTT with household candle wax (Figure 6c,d). The mobility improved significantly from 0.6[1] to 1.8 cm^2 V^{-1} s^{-1} at 60 wt% of household candle wax. Accordingly, incorporation of a nonpolar, incompatible hydrocarbon binder into a D–A polymer semiconductor composition was a reliable and powerful approach

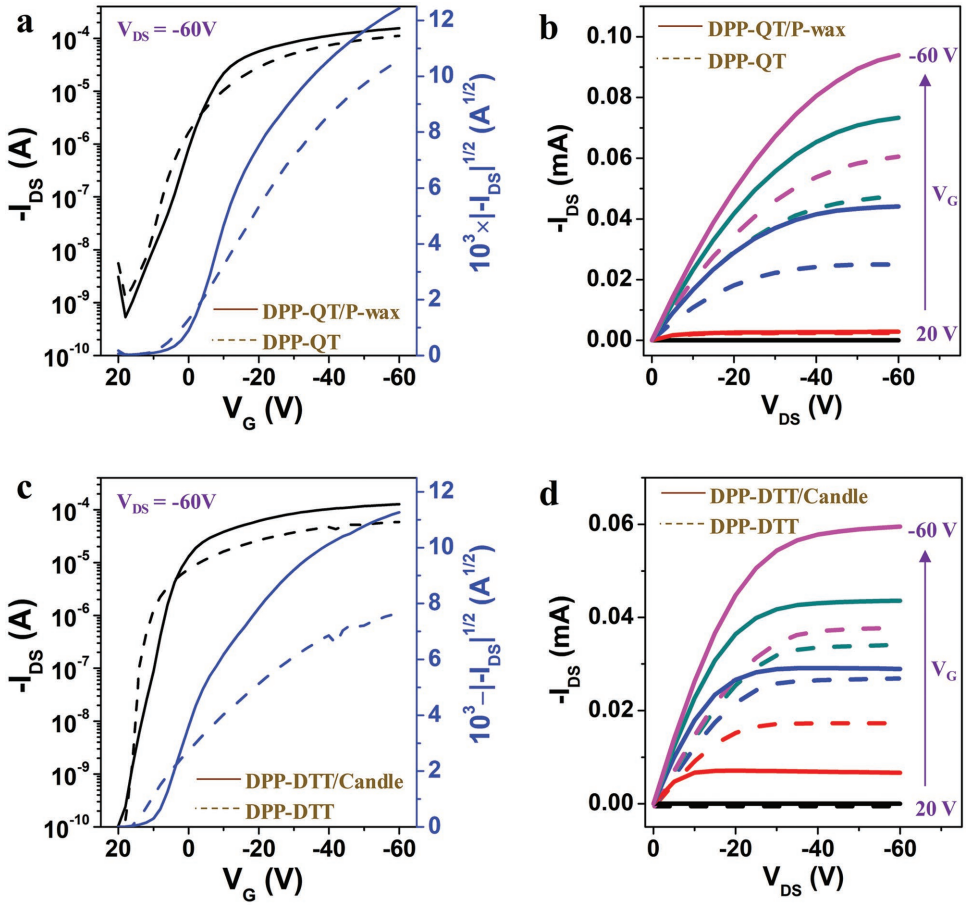

Figure 6. a,c) Transfer characteristics and b,d) output curves of OFETs with other polymer semiconductors and hydrocarbon binders without postdeposition thermal annealing: a,b) neat DPP-QT and DPP-QT/P-wax composition; c,d) neat DPP-DTT and DPP-DTT/candle composition.

© 2018 WILEY-VCH Verlag GmbH & Co. KGaA, Weinheim

to enhance its OFET performance without the needs for thermal annealing.

3. Conclusion

In conclusion, we have developed an efficient and general approach to solution fabrication of high-performance OFETs at room temperature without the needs for high-temperature thermal annealing. The process involves incorporation of a hydrocarbon wax into a D–A polymer channel semiconductor composition to facilitate phase separation and molecular ordering of D–A polymer semiconductor at room temperature. The resulting channel semiconductor film manifests a continuous semiconductor nanowire network intercalating in a maze of nano/micropore structures. OFETs using channel semiconductors of this nature have afforded practically useful FET mobility of up to about 5 $cm^2 v^{-1} s^{-1}$ and on/off ratio of 10^6 and beyond. They have also exhibited excellent thermal stability. These results therefore represent hitherto benchmark performance for OFETs solution fabricated at room temperature without thermal annealing. We expect the present process to have broad impacts toward the transition of low-cost manufacturing of OFET circuitries from laboratory to marketplace.

4. Experimental Section

Materials: DPP-DTT and DPP-QT D–A polymers were synthesized according to previously reported procedures.[4,9] Parafilm M film, DCB, and octadecyltrichloro-silane (OTS) were purchased from Sigma-Aldrich and used as received. Household candle was purchased from supermarket.

Preparation of Coating Solutions: DPP-DTT and P-wax were first dissolved in DCB at a concentration of 4.0 mg mL^{-1} by heating at 60 °C overnight. The resulting P-wax solution was filtered through a syringe filter before use. The 40:60% by weight solution of DPP-DTT/P-wax was prepared by mixing 40 vol% DPP-DTT solution and 60 vol% P-wax solution to provide the final DPP-DTT/P-wax coating solution. Solutions of DPP-DTT/P-wax of various concentrations were prepared accordingly using appropriate portions of DPP-DTT and P-wax solutions. The DPP-QT/P-wax (40/60% by weight) and DPP-DTT/candle wax (40/60% by weight) solutions were prepared in the same manner.

Film Deposition and Characterization: Heavily doped silicon wafer with an ≈300 nm thick thermally grown SiO_2 was used as substrates. The Si/SiO_2 substrates were cleaned in sequence with acetone, isopropyl alcohol, and deionized water in an ultrasonic bath, followed by blowing dry with nitrogen gas. The cleaned substrates were treated with OTS in accordance with previously reported procedures.[33] The channel semiconductor films were deposited by spin coating at 1500 rpm for 150 s of polymer semiconductor or polymer semiconductor/hydrocarbon binder solutions onto OTS-modified Si/SiO_2 substrates, and then dried in glove box overnight. UV–vis absorption spectra were recorded using an HP 8453 UV-visible Spectrophotometer. The surface morphology of the resulting semiconductor films was characterized with a Veeco Digital instruments AFM instrument. The thickness of the films was measured using a Veeco Dektak 150 Profilometer. The GIXD measurements were conducted at 23A SWAXS beamline at the National Synchrotron Radiation Research Center, Hsinchu, Taiwan, using a 10 keV primary beam, 0.15° incident angle and C9728DK area detector.[34] TGA was carried out on a Perkin Elmer Pyris 1 TGA while DSC measurements was performed on a Netzsch DSC (204F1) instrument. All the samples were heated (or cooled) with a heating (or cooling) rate of 10 °C min^{-1}.

OFET Fabrication and Characterization: OFETs were fabricated on OTS-modified SiO_2/Si wafer substrates with bottom-gate, top-contact configuration. The channel semiconductor layers were deposited as described above. The patterned source/drain electrodes were formed by thermal deposition of ≈60 nm gold through a shadow mask. The channel width (W) was fixed at 1500 µm while the channel length (L) of 80–200 µm was utilized in the measurement. All OFET characterizations were conducted at room temperature in ambient conditions using a Keithley 2636B two channel Source/Meter.

Supporting Information

Supporting Information is available from the Wiley Online Library or from the author.

Acknowledgements

This work was financially supported by a Strategic Development Fund (SDF13-0531-A02) of Hong Kong Baptist University, Hung Hin Shiu Charitable Foundation, and a Collaborative Research Fund (C5015-15GF) from Hong Kong Research Grants Council. The authors also acknowledge the financial support from the Fundamental Research Funds for the Central Universities (SWU117044) and NSFC (Grant Nos. 11204247 and 11404266).

Conflict of Interest

The authors declare no conflict of interest.

Keywords

annealing free, donor–acceptor polymer semiconductor, nanoporous network, organic field-effect transistor, printed electronics

Received: November 2, 2017
Revised: January 15, 2018
Published online:

[1] H. Sirringhaus, T. Kawase, R. H. Friend, T. Shimoda, M. Inbasekaran, W. Wu, E. P. Woo, *Science* **2000**, *290*, 2123.
[2] I. Kang, H.-J. Yun, D. S. Chung, S.-K. Kwon, Y.-H. Kim, *J. Am. Chem. Soc.* **2013**, *135*, 14896.
[3] H. Chen, Y. Guo, G. Yu, Y. Zhao, J. Zhang, D. Gao, H. Liu, Y. Liu, *Adv. Mater.* **2012**, *24*, 4618.
[4] J. Li, Y. Zhao, H. S. Tan, Y. Guo, C.-A. Di, G. Yu, Y. Liu, M. Lin, S. H. Lim, Y. Zhou, H. Su, B. S. Ong, *Sci. Rep.* **2012**, *2*, 754.
[5] S. Wang, M. Kappl, I. Liebewirth, M. Müller, K. Kirchhoff, W. Pisula, K. Müllen, *Adv. Mater.* **2012**, *24*, 417.
[6] C.-a. Di, K. Lu, L. Zhang, Y. Liu, Y. Guo, X. Sun, Y. Wen, G. Yu, D. Zhu, *Adv. Mater.* **2012**, *22*, 1273.
[7] G. Kim, S.-J. Kang, G. K. Dutta, Y.-K. Han, T. J. Shin, Y.-Y. Noh, C. Yang, *J. Am. Chem. Soc.* **2014**, *136*, 9477.
[8] H. Pan, Y. Li, Y. Wu, P. Liu, B. S. Ong, S. Zhu, G. Xu, *J. Am. Chem. Soc.* **2007**, *129*, 4112.
[9] Y. Li, P. Sonar, S. P. Singh, M. S. Soh, M. van Meurs, J. Tan, *J. Am. Chem. Soc.* **2011**, *133*, 2198.
[10] C.-J. Chiang, J.-C. Chen, H.-Y. Tsao, K.-Y. Wu, C.-L. Wang, *Adv. Funct. Mater.* **2015**, *25*, 606.
[11] D. Khim, K.-J. Baeg, J. Kim, M. Kang, S.-H. Lee, Z. Chen, A. Facchetti, D.-Y. Kim, Y.-Y. Noh, *ACS Appl. Mater. Interfaces* **2013**, *5*, 10745.

© 2018 WILEY-VCH Verlag GmbH & Co. KGaA, Weinheim

[12] D. Bharti, V. Raghuwanshi, I. Varun, A. K. Mahato, S. P. Tiwari, *ACS Appl. Mater. Interfaces* **2017**, *9*, 26226.
[13] C. Luo, A. K. K. Kyaw, L. A. Perez, S. N. Patel, M. Wang, G. C. Bazan, E. J. Kramer, A. J. Heeger, *Nano Lett.* **2014**, *14*, 2764.
[14] H.-R. Tseng, H. Phan, C. Luo, M. Wang, L. A. Perez, S. N. Patel, L. Ying, E. J. Kramer, T.-Q. Nguyen, G. C. Bazan, A. J. Heeger, *Adv. Mater.* **2014**, *26*, 2993.
[15] F. Zhang, X. Dai, W. Zhu, H. Chung, Y. Diao, *Adv. Mater.* **2017**, *29*, 1700411.
[16] F.-J. Lin, C. Guo, W.-T. Chuang, C.-L. Wang, Q. Wang, H. Liu, C.-S. Hsu, L. Jiang, *Adv. Mater.* **2017**, *29*, 1606987.
[17] S. Goffri, C. Müller, N. Stingelin-Stutzmann, D. W. Breiby, C. P. Radano, J. W. Andreasen, R. Thompson, R. A. J. Janssen, M. M. Nielsen, P. Smith, H. Sirringhaus, *Nat. Mater.* **2006**, *5*, 950.
[18] A. C. Arias, F. Endicott, R. A. Street, *Adv. Mater.* **2006**, *18*, 2900.
[19] L. Qiu, J. A. Lim, X. Wang, W. H. Lee, M. Hwang, K. Cho. *Adv. Mater.* **2008**, *20*, 1141.
[20] Y. Yuan, G. Giri, A. L. Ayzner, A. P. Zoombelt, S. C. B. Mannsfeld, J. Chen, D. Nordlund, M. F. Toney, J. Huang, Z. Bao, *Nat. Commun.* **2014**, *5*, 3005.
[21] L. Qiu, W. H. Lee, X. Wang, J. S. Kim, J. A. Lim, D. Kwak, S. Lee, K. Cho, *Adv. Mater.* **2009**, *21*, 1349.
[22] Y. Kimura, T. Nagase, T. Kobayashi, A. Hamaguchi, Y. Ikeda, T. Shiro, K. Takimiya, H. Naito, *Adv. Mater.* **2015**, *27*, 727.
[23] Y. Lei, P. Deng, J. Li, M. Lin, F. Zhu, T.-W. Ng, C.-S. Lee, B. S. Ong, *Sci. Rep.* **2016**, *6*, 24476.
[24] Y. Lei, P. Deng, M. Lin, X. Zheng, F. Zhu, B. S. Ong, *Adv. Mater.* **2016**, *28*, 6687.
[25] F. G. del Pozo, S. Fabiano, R. Pfattner, S. Georgakopoulos, S. Galindo, X. Liu, S. Braun, M. Fahlman, J. Veciana, C. Rovira, X. Crispin, M. Berggren, M. Mas-Torrent, *Adv. Funct. Mater.* **2016**, *26*, 2379.
[26] S. Galindo, A. Tamayo, F. Leonardi, M. Mas-Torrent, *Adv. Funct. Mater.* **2017**, *27*, 1700526.
[27] H. Sirringhaus, *Adv. Mater.* **2014**, *26*, 1319.
[28] P. J. Brown, D. S. Thomas, A. Köhler, J. S. Wilson, J.-S. Kim, *Phys. Rev. B* **2003**, *67*, 064203.
[29] B. S. Ong, Y. Wu, P. Liu, S. Gardner, *Adv. Mater.* **2005**, *17*, 1141.
[30] S. Y. Son, Y. Kim, J. Lee, G.-Y. Lee, W.-T. Park, Y.-Y. Noh, C. E. Park, T. Park, *J. Am. Chem. Soc.* **2016**, *138*, 8096.
[31] B. C. Schroeder, T. Kurosawa, T. Fu, Y.-C. Chiu, J. Mun, G.-J. N. Wang, X. Gu, L. Shaw, J. W. E. Kneller, T. Kreouzis, M. F. Toney, Z. Bao, *Adv. Funct. Mater.* **2017**, *27*, 1701937.
[32] J. H. Lee, Y. H. Lee, Y. H. H, J. Kwon, S. Pyo, Y.-H. Kim, W. H. Lee, *RSC Adv.* **2017**, *7*, 7526.
[33] Y. Lei, W. Bo, W. K. E. Chan, F. Zhu, B. S. Ong, *J. Mater. Chem. C* **2015**, *3*, 12267.
[34] J. Mai, H. Lu, T.-K. Lau, S.-H. Peng, C.-S. Hsu, W. Hua, N. Zhao, X. Xiao, X. H. Lu, *J. Mater. Chem. A* **2017**, *5*, 11739.

© 2018 WILEY-VCH Verlag GmbH & Co. KGaA, Weinheim